

# A Comparative Study of Lectin Affinity Based Plant *N*-Glycoproteome Profiling Using Tomato Fruit as a Model\*<sup>§</sup>

Elie Ruiz-May<sup>‡</sup>, Simon Hucko<sup>§</sup>, Kevin J. Howe<sup>§</sup>, Sheng Zhang<sup>¶</sup>,  
Robert W. Sherwood<sup>¶</sup>, Theodore W. Thannhauser<sup>§</sup>, and Jocelyn K. C. Rose<sup>‡</sup>||

Lectin affinity chromatography (LAC) can provide a valuable front-end enrichment strategy for the study of *N*-glycoproteins and has been used to characterize a broad range eukaryotic *N*-glycoproteomes. Moreover, studies with mammalian systems have suggested that the use of multiple lectins with different affinities can be particularly effective. A multi-lectin approach has also been reported to provide a significant benefit for the analysis of plant *N*-glycoproteins; however, it has yet to be determined whether certain lectins, or combinations of lectins are optimal for plant *N*-glycoproteome profiling; or whether specific lectins show preferential association with particular *N*-glycosylation sites or *N*-glycan structures. We describe here a comparative study of three mannose-binding lectins, concanavalin A, snowdrop lectin, and lentil lectin, to profile the *N*-glycoproteome of mature green stage tomato (*Solanum lycopersicum*) fruit pericarp. Through coupling lectin affinity chromatography with a shotgun proteomics strategy, we identified 448 putative *N*-glycoproteins, whereas a parallel lectin affinity chromatography plus hydrophilic interaction chromatography analysis revealed 318 putative *N*-glycosylation sites on 230 *N*-glycoproteins, of which 100 overlapped with the shotgun analysis, as well as 17 *N*-glycan structures. The use of multiple lectins substantially increased *N*-glycoproteome coverage and although there were no discernible differences in the structures of *N*-glycans, or the charge, isoelectric point (pI) or hydrophobicity of the glycopeptides that differentially bound to each lectin, differences were observed in the amino acid frequency at the -1 and +1 subsites of the *N*-glycosylation sites. We also demonstrated an alternative and complementary *in planta* recombinant expression strategy, followed by affinity MS

analysis, to identify the putative *N*-glycan structures of glycoproteins whose abundance is too low to be readily determined by a shotgun approach, and/or combined with deglycosylation for predicted deamidated sites, using a xyloglucan-specific endoglucanase inhibitor protein as an example. *Molecular & Cellular Proteomics* 13: 10.1074/mcp.M113.028969, 566–579, 2014.

*N*-glycosylation is one of the most heterogeneous and common post-translational modifications of eukaryotic proteins and one that affects many aspects of protein targeting, enzymatic properties, stability and intermolecular interactions (1–3). There is therefore considerable interest in developing robust and sensitive high throughput analytical pipelines to isolate and structurally characterize *N*-glycoprotein populations (2, 4–8), allowing glycoprotein identification and analysis of the glycosylation site occupancy and *N*-glycan structure. To this end, lectin affinity chromatography (LAC)<sup>1</sup> is increasingly popular: specifically, various lectins are known to have different binding affinities for *N*-glycans and so the selective binding of *N*-glycoproteins in complex protein extracts to these lectins and their subsequent release allows a critical enrichment step before sequencing and glycan analysis by MS (9).

As a refinement of this approach, the use of multiple lectin affinity chromatography (MLAC) in yeast and animal studies (4, 6, 10), using different proteomic platforms, has been shown to increase the numbers of isolated *N*-glycoproteins or *N*-glycopeptides. Collectively, these studies of taxonomically diverse eukaryotic *N*-glycoproteomes suggest a general conservation of the glycosylation site (N-X-S/T, where X can be any amino acid except proline), as well as conserved features of three-

From the <sup>‡</sup>Department of Plant Biology, Cornell University, Ithaca, New York 14853; <sup>§</sup>USDA-ARS, Robert W. Holley Center for Agriculture and Health, Ithaca, New York 14853; <sup>¶</sup>Proteomics and Mass Spectrometry Facility, Institute of Biotechnology, Ithaca, New York 14853

Received March 5, 2013, and in revised form, October 20, 2013

Published, MCP Papers in Press, November 6, 2013, DOI 10.1074/mcp.M113.028969

Author contributions: E.R., S.Z., and J.K.R. designed research; E.R., S.H., K.J.H., and R.W.S. performed research; E.R., S.H., K.J.H., S.Z., R.W.S., T.W.T., and J.K.R. analyzed data; E.R., S.Z., T.W.T., and J.K.R. wrote the paper.

<sup>1</sup> The abbreviations used are: LAC, Lectin affinity chromatography; ConA, concanavalin A; ER, endoplasmic reticulum; GNA, snowdrop lectin; GA, Golgi apparatus; GH, glycosyl hydrolase; HILIC, hydrophilic interaction chromatography; LCH, lentil lectin; MS, mass spectrometry; MLAC, multiple lectin affinity chromatography; MG, mature green MG; PGC, porous graphite carbon; PG, polygalacturonase; PME, pectin methylesterase; RLKs, receptor-like kinases; RP, reverse phase; SP, Signal peptide; XTHs, xyloglucan endotransglucosylase/hydrolases; XEGIP, xyloglucan-specific endoglucanase inhibitor protein; PI-IDA, Precursor ion scanning-triggered information dependent acquisition.

dimensional protein structure (4, 6, 10). Although there have been several studies to determine the structural basis of the binding specificity of specific lectins to yeast and animal *N*-glycoproteins (11), larger scale *N*-glycoproteomic analyses have typically not attempted to determine whether a particular combination of lectins provides optimal enrichment, or whether specific features, such as *N*-glycan structure or amino acid sequence at and around the *N*-glycosylation site, are associated with different lectins. Therefore, systematic comparative studies are essential to determine whether particular lectins can be optimal for specific tissues, organs, and organisms.

LAC has also been used in plant *N*-glycoprotein analyses to enrich for populations of cell wall localized proteins (8, 12, 13) and a recent report (13) described the application of MLAC to map substantial numbers of *N*-glycosylation sites in a range of key experimental model organisms, included the plant *Arabidopsis thaliana*. Using a LTQ-Orbitrap Velos mass spectrometer, the authors identified 2186 unique *N*-glycosylation sites in proteins extracted from five different *Arabidopsis* organs (13), which represents a substantial increase in the number of identified *N*-glycosylation sites that have resulted from previous plant *N*-glycoprotein studies. However, the particular analytical platform that was used did not allow the structural characterization of the *N*-glycans or *N*-glycopeptides (13). Indeed, certain features of *N*-glycopeptides, such as poor fragmentation, heterogeneity and a large dynamic range in most complex mixtures often limits the structural analysis of *N*-glycans in high throughput systematic analyses (2). It is also important to note that the structures of plant *N*-glycans differ from those of animals and yeast, as exemplified by the presence of  $\beta$ -1, 2-xylose and  $\alpha$ -1, 3-fucose and the complete absence of multiantennary *N*-glycans and sialic acid in plant *N*-glycoproteins (1, 14). Therefore, assumptions that are made with regard to the lectin binding of animal and yeast proteins do not necessarily apply to those from plants. Consequently, there is a need to investigate the structural basis of lectin binding to plant *N*-glycoproteins. Moreover, the limitations of typical shotgun based profiling approaches in identifying and characterizing low abundance *N*-glycoproteins in complex protein extracts need to be addressed to allow more comprehensive plant *N*-glycoproteome profiling.

In the present study we address both these issues using mature green stage tomato (*Solanum lycopersicum*) fruit pericarp as an experimental model to carry out a comparative analysis of *N*-glycoproteins associated with each of three mannose-binding lectins: concanavalin A (ConA), snowdrop lectin (GNA), and lentil lectin (LCH). Fruit development is associated with substantial cell wall metabolism and the expression of many wall localized *N*-glycoproteins (8) and tomato in particular represents an excellent model for studies of fleshy fruits and cell wall *N*-glycoproteins (15). We established an MLAC analytical pipeline that included shotgun proteomic profiling and deglycosylation and deamidation analysis, to allow the determination of *N*-glycoprotein protein identity,

*N*-glycosylation site and *N*-glycan structures. This information was then used to establish whether a combination of lectins is indeed advantageous for the study of plant *N*-glycoproteomes, and to assess whether any of these structural characteristics result in predictable preferential binding to specific lectins. From these studies it became evident that large dynamic range of *N*-glycoprotein abundance was a significant limiting factor in the structural determination of the tomato, and that there was a bias toward the detection of highly abundant *N*-glycopeptides. We therefore evaluated the use of an *in planta* recombinant expression strategy, combined with affinity purification MS (AP-MS), as a means to characterize the *N*-glycan structures of glycoproteins whose abundance is too low to be readily determined via the primary shotgun pipeline, using a tomato xyloglucan-specific endoglycanase inhibitor protein (XEGIP) as a test case.

#### EXPERIMENTAL PROCEDURES

**Plant Materials**—Tomato (cultivar M82) plants were grown in a greenhouse in Ithaca, New York (16-h of light and 8-h of dark cycle). Fruits were harvested at the mature green (MG) stage when fruits reached full size, but were still green, with no visible signs of ripening. Fruit pericarp tissue from three MG tomato fruits from three different plants was pooled and flash frozen in liquid nitrogen.

**Protein Extraction**—Protein extraction was carried out as previously described (8) with minor modifications. Briefly, 15 g (fresh weight) of frozen pericarp tissue was powdered in liquid nitrogen with a pestle and mortar and then homogenized further with a Powergen hand homogenizer (Fisher Scientific, Ottawa, Canada) for 15 s in three volumes of extraction buffer (25 mM Tris, pH 7.0, 0.2 M CaCl<sub>2</sub>, 0.5 M NaCl, polyvinylpyrrolidone (1 g/10 g fresh weight) and 20  $\mu$ l/g fresh weight of protease inhibitor mixture (Sigma-Aldrich, St. Louis, MO). The resulting suspension was shaken for 2 h at 4 °C, centrifuged at 16,000  $\times$  *g* at 4 °C for 30 min and the supernatant collected for subsequent enrichment of *N*-glycoproteins by lectin affinity chromatography. Protein concentration was determined using the BCA™ Assay Kit (Pierce; Rockford IL) with BSA as a standard.

**Multi Lectin Affinity Chromatography**—Three different mannose-binding lectins were used for *N*-glycoprotein enrichment: concanavalin A (ConA), *Galanthus nivalis* agglutinin (GNA) and *Lens culinaris* agglutinin (LCH). Five milliliter cartridges of resin covalently bound to one of each of the three lectins (Qiagen, Hilden, Germany) were pre-equilibrated with binding buffer (20 mM Tris-HCl pH 7.0, 0.5 M NaCl, 1 mM CaCl<sub>2</sub>, 1 mM MnCl<sub>2</sub>, and 1 mM MgCl<sub>2</sub>), at a flow rate of 0.08 ml/min, and the column washed with ten column volumes of binding buffer. The supernatants from the crude protein extracts described above were loaded onto each of the columns with a peristaltic pump, unbound proteins washed off the column with ten column volumes of binding buffer, or until the absorbance at 280 nm returned to the baseline value. The bound proteins were eluted using an AKTA Explorer liquid chromatography system (GE Healthcare, Piscataway, NJ) with five column volumes of elution buffer (same composition as the binding buffer but additionally, 0.5 M with respect to  $\alpha$ -methyl-D-mannopyranoside (Calbiochem, La Jolla, CA)) at a flow rate of 0.75 ml/min, monitoring the absorbance of the eluent at 280 nm. The protein-containing fraction was concentrated and the eluting buffer was exchanged for 100 mM ammonium bicarbonate, using a 5 kDa cutoff centrifugal concentrator (Amicon Ultra-15, Millipore, Billerica, MA) and then lyophilized. The lyophilized samples were then dissolved in a minimal volume of 8 M urea in 100 mM ammonium bicarbonate. To visualize the protein composition of the crude ex-

tract, as well as the enriched fractions, aliquots (10  $\mu$ g protein) were mixed with 5 $\times$  Laemmli buffer, fractionated on 12% Tris-glycine SDS-PAGE gels (TGX™ gels, Bio-Rad; Hercules, CA) and stained with SYPRO ruby (Invitrogen, Grand Island, NY).

**Trypsin Digestion**—Trypsin digestions were carried out as previously described (8, 12) with slight modifications. Briefly, the samples dissolved in 8 M urea in 100 mM ammonium bicarbonate (100  $\mu$ g protein) were reduced with 10 mM DTT for 1 h and alkylated with 25 mM iodoacetamide in the dark for 30 min, both steps at room temperature, and diluted to a final concentration of 1 M urea with 100 mM ammonium bicarbonate. Proteins were digested with trypsin (Trypsin Gold, Mass Spectrometry Grade, Promega, Madison, WI) at a 1:20 w/w trypsin: protein ratio for 16 h at 37 °C.

***N*-glycopeptides Enrichment**—For enrichment of *N*-glycopeptides, the pool of tryptic peptides were manually passed through a porous graphite carbon (PGC) cartridge (Thermo Scientific, Bellefonte, PA, USA) with a syringe. The PGC cartridge was prepared by sequentially passing through 1 ml 1 M NaOH, 2 ml water, 1 ml 30% acetic acid, 2 ml water, 1 ml elution solvent (50% acetonitrile, 0.1% formic acid [v/v] in water), and 1 ml wash solvent (5% acetonitrile, 0.1% formic acid [v/v] in water). The pH of the trypsinized samples was adjusted to 5.0 with 0.1% trifluoroacetic acid (TFA) and loaded onto the PGC cartridge. Subsequently, 1 ml wash solvent was passed through the column and the flow through containing the nonglycosylated peptides was recovered and desalted with a C18 solid phase extraction cartridge (Waters, Milford, MA). The bound *N*-glycopeptides were eluted with 1 ml elution solvent. The flow through and bound fractions were dried using a SpeedVac (Thermo Savant, Holbrook, NY) for shotgun analysis or *N*-glycosylation analysis in the case of the bound fraction.

**Peptide Fractionation for Shotgun Proteomics**—PGC flow through and bound fractions were additionally fractionated using high pH reverse phase (hpRP) chromatography using an Akta Explorer FPLC equipped with a Frac 950 fraction collector and UV detector (GE Healthcare). Tryptic peptides were reconstituted in buffer A (20 mM ammonium formate, pH 9.5 in water), and loaded onto a Resource RPC 3 ml column (GE Healthcare) with 20 mM ammonium formate, pH 9.5 as buffer A and 80% acetonitrile (ACN)/20 mM ammonium formate as buffer B. The LC was performed using a gradient from 10–45% of buffer B in 30 min, at a flow rate of 200  $\mu$ l/min. Twenty-four fractions were collected from each sample (PGC flow through and bound fractions), of which five were pooled based on the UV absorbance at 214 nm, then dried for subsequent nanoLC-MS/MS analysis.

**Enrichment of Glycopeptides by HILIC and Deglycosylation**—The tryptic peptides of glycoproteins (*i.e.* the PGC bound fraction) were subjected to hydrophilic interaction chromatography (HILIC) to partition glycopeptides and nonglycopeptides. HILIC was carried out using a Dionex UltiMate 3000 high performance LC system with a built-in microfraction collection option in its autosampler and UV detection (Thermo-Dionex, Sunnyvale, CA). The tryptic peptides were reconstituted in 80% ACN containing 0.25% trifluoroacetic acid for ion pair normal phase separation (16) and loaded onto a Polyhydroxyethyl A™ column (5  $\mu$ m, 2.1  $\times$  200 mm, 200 Å, PolyLC, MD) with 10% ACN as eluent A and 90% ACN as eluent B. The LC was performed using a gradient from 90 to 40% eluent B in 30 min at a flow rate of 200  $\mu$ l/min. Forty four fractions were collected at 1 min intervals, pooled into 31 fractions, dried and reconstituted in 100  $\mu$ l of 0.5% formic acid for screening glycopeptides-containing fractions by nanoLC-MS/MS on a 4000 Qtrap operating in the precursor ion (PI) scan-triggered, information dependent analysis (IDA) mode. A quarter (25  $\mu$ l) of the reconstituted fractions containing glycopeptides was further treated with 50 mU of PNGase A at 37 °C for 16 h in 100 mM sodium citrate/sodium phosphate monobasic pH 5.0. The PNGase A treated samples were passed through Omix C18 tips, and reconsti-

tuted in 25  $\mu$ l of 0.2% FA before high resolution MS and MS/MS analysis in LTQ Orbitrap Velos.

**NanoLC-MS/MS Analyses**—High pH RPLC fractions on PGC bound samples and the 5 pooled HILIC fractions treated with PNGase A were analyzed by nanoLC-MS/MS analysis using a LTQ-Orbitrap Velos (Thermo-Fisher Scientific, San Jose, CA) mass spectrometer equipped with a “CorConneX” nano ion source (CorSolutions LLC, Ithaca, NY). The Orbitrap was interfaced with an UltiMate 3000 RSLC system (Dionex, Sunnyvale, CA). Each reconstituted fraction (5  $\mu$ l) was injected onto a PepMap C18 trap column (5  $\mu$ m, 300  $\mu$ m  $\times$  5 mm, Dionex) at 20  $\mu$ l/min flow rate for loading, and then separated on a PepMap C-18 RP nano column (3  $\mu$ m, 75  $\mu$ m  $\times$  15 cm), utilizing a 60 min gradient from 5% to 40% ACN in 0.1% formic acid at 300 nl/min. The eluted peptides were detected by the Orbitrap through the nano ion source containing a 10- $\mu$ m analyte emitter (NewObjective, Woburn, MA). The Orbitrap Velos was operated in positive ion mode with nanospray voltage set at 1.5 kV and source temperature at 275 °C. The calibrants were either the background polysiloxane ion signal at *m/z* 445.120025 as an internal calibrant, or the Ultramark 1621 external calibrant for the Fourier Transform (FT) mass analyzer. The instrument was operated in parallel data-dependent acquisition (DDA) mode using the FT mass analyzer for one survey MS scan at a resolution of 60,000 (fwhm at *m/z* 400) for the mass range of *m/z* 375–1800 for precursor ions, followed by MS/MS scans of the top 7 most intense peaks with multiple charged ions above a threshold ion count of 7500 in both LTQ mass analyzer and HCD-based FT mass analyzer at 7500 resolution. Dynamic exclusion parameters were set at repeat count 1 with a 25 s repeat duration, exclusion list size of 500, 45 s exclusion duration, and  $\pm$ 10 ppm exclusion mass width. Collision induced dissociation (CID) parameters were set at the following values: isolation width 2.0 *m/z*, normalized collision energy 35%, activation Q at 0.25, and activation time 10 ms. The activation time is 0.1 ms for HCD analysis. All data were acquired with Xcalibur 2.1 software (Thermo-Fisher Scientific).

The nanoLC-MS/MS analysis for characterization of glycosylation sites was performed on an UltiMate3000 nanoLC system (Dionex, Sunnyvale, CA) coupled with a hybrid triple quadrupole linear ion trap mass spectrometer, the 4000 Q Trap (AB SCIEX, Framingham, MA). The tryptic peptides in each HILIC fraction (5  $\mu$ l) were injected with an autosampler onto a PepMap C18 trap column (5  $\mu$ m, 300  $\mu$ m  $\times$  5 mm, Dionex) with 0.1% FA at 20  $\mu$ l/min for 1 min, then separated on a PepMap C18 RP nano column (3  $\mu$ m, 75  $\mu$ m  $\times$  15 cm, Dionex) using a 60-min gradient of 10% to 35% ACN in 0.1% FA at 300 nl/min, followed by a 3-min ramp to 95% ACN-0.1% formic acid and a 5-min hold at 95% ACN-0.1% FA. MS data acquisition was performed using Analyst 1.4.2 software (AB Sciex, Foster City, CA) for PI scan-triggered IDA analysis. The precursor ion scan of the oxonium ion (HexNAc<sup>+</sup> at *m/z* 204.08) was monitored using a step size of 0.2 Da across a mass range of *m/z* 500–1600 and the parameters were set as reported previously (18). For IDA analysis, each precursor ion scan was followed by one enhanced resolution scan and the two highest intensity ions with multiple charge states were selected for MS/MS using rolling collision energy that was set based on the charge state and *m/z* value of each ion.

**Data Analysis and Interpretation**—All of the DDA raw data from the Orbitrap were converted into MGF files using Proteome Discoverer 1.3 (PD1.3, Thermo). The subsequent searches were carried out using Mascot Daemon (version 2.3, Matrix Science, Boston, MA) with the following search parameters: semitryptic protease specificity, one missed cleavage allowed, 20 ppm precursor mass tolerance, 0.8 Da for CID and 0.05 Da for HCD fragment ion mass tolerance with a fixed modification of cysteine carbamidomethylation, and variable modifications of methionine oxidation and asparagine and glutamine deamidation. Mass spectra were used to search a translated custom uni-

gene database ([ftp://ted.bti.cornell.edu/pub/tomato\\_454\\_unigene](ftp://ted.bti.cornell.edu/pub/tomato_454_unigene)) derived from tomato RNA-Seq data generated with 454 reads (454 pyrosequencing; GS FLX, Roche, Indianapolis, IN) from different tomato tissues (fruit, leaves, pollen, styles). The RNA-Seq database combined with the SGN expressed sequence tag (EST) collection (<http://solgenomics.net/bulk/input.pl?mode=ftp>) are described in detail in Lopez-Casado *et al.*, (19). Spectral data were also searched against a version of the tomato database described above in which the sequences were reversed, and the resulting matches used to estimate false-positive rates. Only peptides that matched with a MASCOT score above the 95% confidence interval threshold ( $p < 0.05$ , MASCOT score  $\geq 44$ ) were considered for protein identification. In cases where the protein was identified by a single peptide match, the threshold was set at a 99% confidence interval (MASCOT score  $\geq 51$ ). These MASCOT scores resulted in a false-positive identification rate of 4.56% at the peptide level. Only proteins containing at least one unique peptide (a sequence that had not been previously assigned to a different protein) were considered. The N to D deamidation found in the N-X-S/T motif, where X is any amino acid except proline, was required for identification of *N*-glycosylation sites. For those identified sites from initial database search, the raw MS/MS spectra were manually inspected and identifications of the peptide with deamidation were confirmed. For peptides containing multiple N-X-S/T motifs, the sites of modification were also manually inspected and validated based on MS/MS fragment ions.

**Determination of XEGIP *N*-glycan Structures and Endogenous Glycopeptides**—The full-length open reading frame of XEGIP (Genbank accession AAN87262) was amplified by PCR using primers containing *att* recombination sites (forward, 5'-ggggacaagttgtacaaaaagcag-gcttcattgcttctctcaattgtttacatgc-3' and reverse, 5'-ggggaccacttgtacaagaaagctgggtcatcaattgaagtgaattaaaattgca-3'), iProof<sup>TM</sup> high-fidelity DNA polymerase (Bio-Rad) and a ripe stage tomato fruit cDNA library as template, generated in the HybriZAP-2.1 vector system (Stratagene, La Jolla, CA). The PCR products were gel purified and then cloned into the pDONR221 vector by overnight incubation in the presence of Gateway BP clonase (Invitrogen) at 25 °C, according to the manufacturer's instructions. The positive entry clones were then introduced into pYL436 destination vector, thereby forming an in-frame C-terminal fusion with a TAP tag (20). Transient expression of the recombinant protein in *Nicotiana benthamiana* leaves with *A. tumefaciens* was performed as described previously (21) except that strain GV2260 was used. After a 72 h incubation under constant illumination at 25 °C, 30 g of infiltrated *N. benthamiana* leaves were collected, powdered in liquid nitrogen using a pestle and mortar, suspended in three volumes of extraction buffer (50 mM Tris-HCl pH 7.5, 150 mM NaCl, 10% glycerol, 0.1% Triton X-100, 1 mM PMSF, and 20  $\mu$ l protease inhibitor mixture [Bio-Rad] per 1 g of fresh tissue), and homogenized for 30 s using a Powered homogenizer (Fisher Scientific, Ottawa, Canada) (8). The resulting suspension was filtered through four layers of Miracloth (Calbiochem, La Jolla, CA) and centrifuged at 15,000  $\times g$  for 30 min at 4 °C. The supernatant was incubated with 500  $\mu$ l of IgG beads (GE Healthcare) that had previously been washed with extraction buffer, for 2 h at 4 °C with gentle rotation. After centrifugation at 1500  $\times g$  for 3 min at 4 °C, the IgG beads were recovered and washed three times with 10 ml of washing buffer (50 mM Tris-HCl pH 7.5, 150 mM NaCl, 10% glycerol, 0.1% Triton X-100). The recombinant XEGIP was eluted from the beads with acidic buffer (glycine-HCl pH 3.0, 0.1% Triton X-100, and 150 mM NaCl).

The purified recombinant XEGIP was fractionated on 12% Tris-glycine SDS-PAGE gels (TGX<sup>TM</sup> gels, Bio-Rad) and stained with Coomassie brilliant blue R-250 (Calbiochem, Darmstadt, Germany). The XEGIP protein band was excised from the gel and digested with trypsin, as described above. The resulting in-gel extracted tryptic

peptides were subjected to PI scan-triggered IDA analysis in 4000 Q Trap as described above.

**Bioinformatic Analysis**—All identified proteins were first screened for the predicted presence of an N-terminal endoplasmic reticulum (ER) targeting signal peptide (SP), using the Signal P 4.1 program (20), because it is required for the cotranslational translocation of the *N*-glycoproteins into the ER, where the *N*-glycans are first added (23). Those with a predicted SP were analyzed for the presence of predicted *N*-glycosylation sites using the NetGlyc 1.0 server (<http://www.cbs.dtu.dk/services/NetNGlyc/>). *N*-glycoproteins were grouped into families using the Pfam data base (24) and functionally classified according to Jamet *et al.*, (25). PSORT (26) and Target P (27) were used to determine the predicted subcellular locations of the identified proteins, and the TMHMM Server v. 2.0 (28) and SOSUI (29) were used to predict transmembrane domains. WebLogo 3 (30) was used to create relative frequency plots of the *N*-glycosylation sequon (N-X-S/T) in the identified *N*-glycopeptides.

## RESULTS

**Workflow and Experimental Design**—The main objective of this study was to determine whether the use of multiple lectins can substantially increase plant *N*-glycoproteome coverage and whether there is any bias to the structures of *N*-glycans or different biochemical properties of glycoproteins that differentially bind to each lectin. We established an analytical workflow (Fig. 1) to compare the efficacy of 3 mannose-binding lectins (ConA, GNA and LCH) as a means to identify glycoproteins from mature green (MG) stage tomato fruit pericarp. The workflow started with  $\sim 300 \mu$ g of *N*-glycoproteins being isolated using each lectin from 15 g (fresh weight) of mature green (MG) stage tomato fruit pericarp. After tryptic digestion of enriched glycoproteins, the PGC-based fractionation was applied for separation of the nonglycopeptide pool (flow through fraction) from the glycopeptide pool (bound fraction). Aliquots of both fractions were further fractionated using high pH reverse phase (hpRP) chromatography, followed by nanoLC-MS/MS analysis for glycoprotein identification, which served as the protein database for the *in silico* enzymatic digest that facilitated the identification of glycosylation sites (as described below).

In a parallel analysis, PGC bound fractions were further fractionated using ion-pairing HILIC for glycopeptide enrichment [14]. We then incorporated PI scan-driven IDA to selectively identify and structurally characterize the glycopeptides, glycosylation sites, and glycoforms with the assistance of the *in silico* tool for all HILIC fractions. The identified glycopeptides and occupancy of each glycosylation site were determined after treatment of five pooled HILIC fractions with PNGase A and subsequent MS/MS analysis on a high resolution instrument capable of distinguishing between peptides incorporating an Asp (glycoform) or an Asn (native amide) (31). In addition, comparative bioinformatic analysis was performed for the data acquired from the shotgun proteomic and direct glycosylation analysis approaches on three different lectins samples. Finally, we used the AP-MS approach to successfully characterize a low abundance glycoprotein (XEGIP), for which a glycopeptide was not identified by our

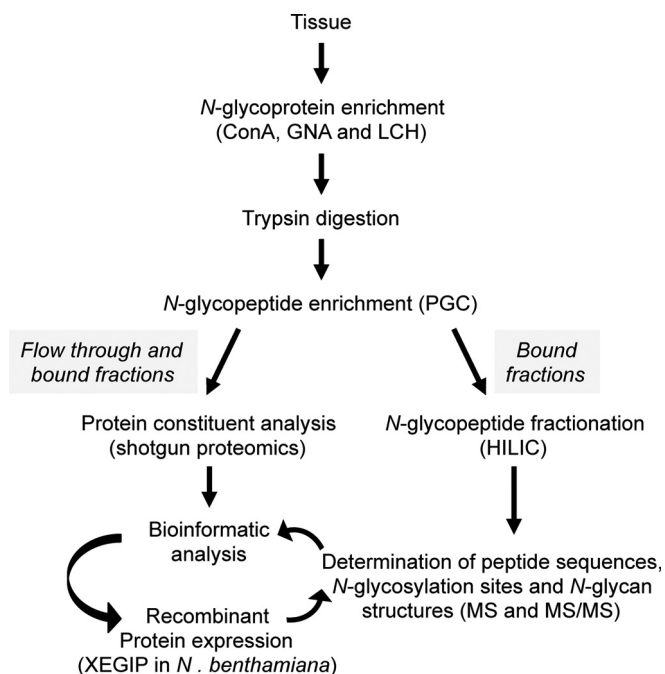


**FIG. 1. Experimental workflow used in this study.** *N*-glycoproteins from tomato fruit pericarp were bound to three different mannose-binding lectins (Concanavalin A, ConA; Snowdrop lectin, GNA; and Lentil lectin, LCH). After trypsin digestion *N*-glycopeptides were fractionated using graphitic carbon (PGC) chromatography. Peptides bound to the PGC column, or present in the flow through, were analyzed by shotgun ESI-MS sequencing. Peptides bound to PGC were further fractionated by hydrophilic interaction chromatography (HILIC). Five main fractions were collected and divided into two aliquots for subsequent identification of *N*-glycosylation sites and analysis of intact *N*-glycopeptides. After bioinformatics analysis, a low abundant glycoprotein (XEGIP) was selected for recombinant expression *in planta* followed by purification and MS analysis to determine the *N*-glycan structures.

precursor ion scan analysis, but rather only nonglycosylated peptides via the shotgun approach.

**Multiple Lectin Affinity Chromatography and Shotgun Proteomics**—Samples of each of the three lectin binding *N*-glycoprotein extracts were also fractionated by SDS-PAGE and visualized by SYPRO ruby staining (Fig. 2A) before trypsin digestion. Although the composition of the total applied protein and flow through samples for the three lectins were not readily distinguishable by this analysis (Fig. 2A, where the ConA flow through is shown), substantial differences were seen in the banding patterns associated with glycoproteins that bound to each lectin, indicating diversity in the binding affinities among the three lectins.

After the enrichment of *N*-glycoproteins by MLAC and trypsin digestion, the next step in our workflow was the enrichment of *N*-glycopeptides by PGC chromatography (Fig. 1). In addition, we analyzed both unbound and bound peptide fractions by shotgun MS/MS to obtain a broad overview of the respective protein populations. Most of the peptides were identified in the bound fraction (peptides attached to PGC) and only 7% in the flow through fractions (unbound peptide),

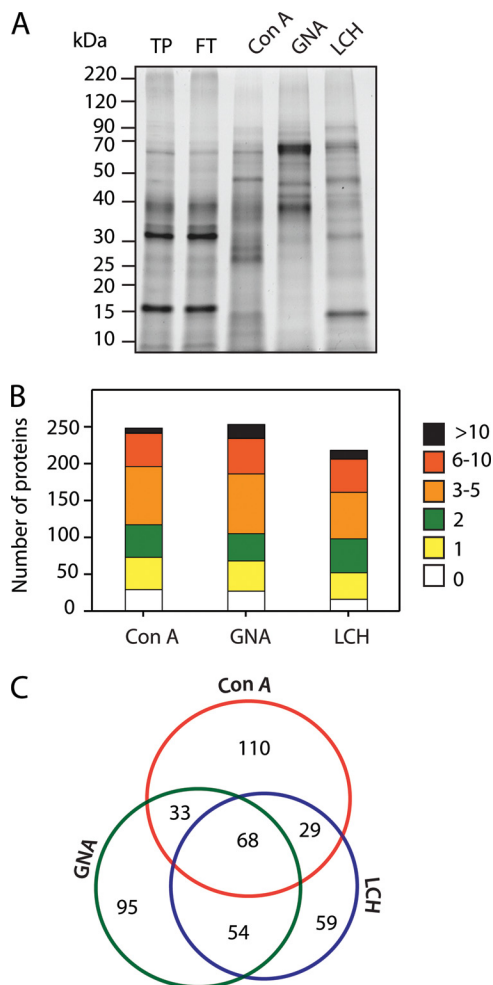


**FIG. 2. Lectin affinity enrichment and identification of *N*-glycoproteins from tomato fruit pericarp.** A, SYPRO ruby stained SDS-PAGE gel of proteins bound to each lectin (ConA, GNA, and LCH). B, identification of glycoproteins using a shotgun MS/MS approach. The numbers of predicted *N*-glycosylation sites in each of the lectin binding glycoprotein fractions are indicated. C, Venn diagram of the glycoproteins identified through shotgun sequencing associated with each of the three lectins.

except in the case of the ConA fractions where 38% were identified in the unbound fraction (supplemental Fig. S1). To match the mass spectra with corresponding gene sequences and identify the proteins, we used two tomato databases: one derived from RNA-seq data to give a large unigene set and the Sol Genomics Network database (<http://solgenomics.net>), as described under “Experimental Procedures”. Only proteins with a predicted N-terminal ER targeting signal peptide (SP; determined using Signal P 4.1, [www.cbs.dtu.dk/services/SignalP](http://www.cbs.dtu.dk/services/SignalP)) were considered further in this study because an SP is required for the cotranslational translocation of nascent proteins into the ER before *N*-glycosylation (23). MS/MS analysis using an LTQ-Orbitrap Velos resulted in the identification of 448 putative *N*-glycoproteins with 240, 251, and 210 putative *N*-glycoproteins in ConA, GNA, and LCH fractions, re-

spectively (Fig. 2B, 2C, supplemental Table S1). The number of predicted *N*-glycosylation sites showed no apparent correlation with the lectin used (Fig. 2B) and in all three cases most of the proteins were predicted to have 3–10 *N*-glycosylation sites, whereas only 12%, 10%, and 8% in the ConA, GNA and LCH fractions, respectively, had no such sites. An apparent complementary nature of the three lectins in the *N*-glycoproteome analysis is suggested by the observation that only 15% (32) of the proteins were identified in all three lectin binding fractions (Fig. 2C), whereas 25% (ConA), 21% (GNA), and 13% (LCH), were specifically associated with one lectin. Of the identified proteins without a predicted SP, and which therefore likely correspond to nonglycosylated “contaminants,” a large proportion were associated with all or multiple lectins and only 14 (5%), 17 (6%), and 4 (2%) were associated with ConA, GNA, and LCH fractions, respectively (supplemental Fig. S2). Cytoplasmic proteins, such as the ribosomal proteins, proteasome subunits and heat shock proteins that were commonly detected in the shotgun analysis did not show specific affinity to a particular lectin (supplemental Fig. S2, supplemental Table S6).

It should be noted that the protein ID lists from above shotgun analysis were used to generate a small target database (instead of the entire tomato database) facilitating the prediction of the masses of all core peptides containing the *N*-linked motif through our in-house developed script. Thus the script served as an *in silico* bioinformatic tool to significantly reduced the number of downstream candidate peptides for discovery screening.

**Deamidation Mapping of *N*-glycosylation Sites in Tomato Fruit Glycoproteins**—In addition to identifying glycoproteins through the shotgun approach, a deamidation analysis was performed to identify the glycosylation sites on the associated glycopeptides. This involved treating the samples with PNGase A, which cleaves *N*-glycans with  $\alpha$ -1,3-fucose (Fuc) at the 3-position of the innermost GlcNAc, as is common in plant *N*-glycans (33, 34). This deglycosylation induces a mass change at the glycosylation site by converting Asn to Asp, which results in a mass shift of 0.9840 Da that can be readily identified by LC-MS/MS analysis (31). However, because spontaneous nonenzymatic deamidation can occur (31, 35), we considered only those cases that also had canonical *N*-glycosylation N-X-S/T sequons.

In total, 318 putative *N*-glycosylation sites were identified, corresponding to 230 *N*-glycoproteins with both predicted *N*-glycosylation sites and a predicted SP (Fig. 3A, supplemental Table S2). Specifically, we identified 131 *N*-glycosylation sites in glycopeptides corresponding to 107 *N*-glycoproteins enriched with ConA, 184 sites corresponding to 134 *N*-glycoproteins with GNA, and 212 *N*-glycosylation sites corresponding to 158 *N*-glycoproteins with LCH (Fig. 3A, supplemental Table S2). Each lectin was associated with a substantial number of glycopeptides that were lectin specific (ConA, 14%; GNA, 16%; LCH, 26%) and only 20% of the

glycopeptides were identified with all three lectins (Fig. 3A), further suggesting the value of lectin multiplexing to increase glycoproteome coverage. A comparison of the mean grand average of hydropathicity (GRAVY) index score, isoelectric point (pI), and molecular weight (Mw) of the *N*-glycopeptides enriched with ConA, GNA, and LCH, showed a similar distribution (Fig. 3B, supplemental Table S3) and a Wilcoxon/Kruskal-Wallis rank sums test indicated no statistically significant correlation between these particular characteristics and the lectin used. Most of the glycopeptides had a low average GRAVY score, consistent with expectations for solvent exposure, and the relatively high proportion of *N*-glycosylation sites in loop and turn regions on the protein surfaces (4, 13).

To determine whether the amino acid sequences of the glycosylation sites influenced the specificity of lectin binding, we compared the position-specific amino acid frequencies of the sequence surrounding the glycosylated Asn in the sequon N-X-S/T, considering six amino acids either side (Fig. 3C and 3D). In all cases, threonine (T) occurred more frequently (1.2-fold) than serine (S) at the second position, consistent with *N*-glycosylation sites mapped in a taxonomically broad range of eukaryotes (4, 6, 10, 13). Proline (P) was absent in the +2 subsite and rare in the +3 position (0.05%) whereas leucine (L) and glycine (G) were over represented in the +2 subsite. When considering all the *N*-glycopeptides associated with each lectin, no clear lectin related differences were apparent (Fig. 3C). However, when analysis was performed of those peptides that were unique to each lectin, then some differences were observed. For example, L and then isoleucine (I) and alanine (A) were the most common amino acids at the –1 subsite when considering all glycosites for all three lectins (Fig. 3C), and also for ConA specific glycosites (Fig. 3D), but were not among the most common 4 amino acids with GNA-specific glycopeptides. Differences were similarly seen at the +1 subsite, where GNA- and LCH-specific peptides showed a different frequency of the most common amino acids.

**Identification of *N*-linked Glycosylation Sites and Glycoforms**—To assess whether differences in *N*-glycan structures might explain the binding of distinct populations of glycopeptides to each of the three lectins, we analyzed each HILIC fraction by precursor ion (PI) scan-driven information dependent analysis (IDA) to selectively detect glycan-containing peptide ions containing the characteristic oxonium ion of *N*-acetylhexosamine (HexNAc) at *m/z* 204.1. This allowed us to determine glycan composition and structural information, peptide sequence and the glycosylation site. To determine the glycosylation site and glycan compositions, we used the detection of a distinct  $Y_1$  ion (with the innermost GlcNAc residue attached to the peptide), which is often one of the most abundant Y type product ions observed in the glycopeptide fragmentation (36–38) and other high *m/z* Y-type fragment ions, allowing us to readily determine the charge state of the  $Y_1$  ion acquired even with the relatively low resolution Q Trap instrument. As a result, we were able to determine the *m/z* of

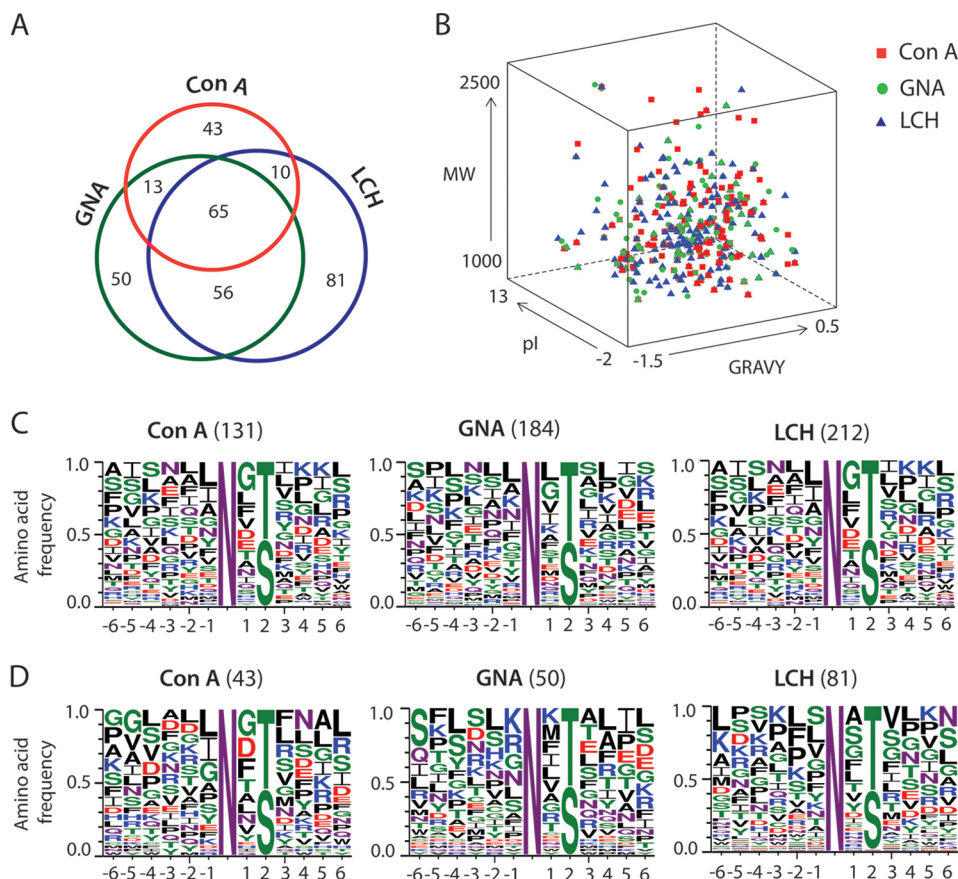


**FIG. 3. Evaluation of glycopeptides associated with each of the three lectins used in the study based on deamination analysis.** *A*, Venn diagram showing the number of *N*-glycopeptides. *B*, distribution of the average GRAVY score, pI (isoelectric point) and Mw (Molecular weight) of the *N*-glycopeptides. *C*, relative frequency plots of the *N*-glycosylation sequon (N-X-S/T) in the entire population of *N*-glycopeptides indicated by the deamination analysis. *D*, relative frequency plots of the *N*-glycosylation sequon (N-X-S/T) indicating the subsets of *N*-glycopeptides that were uniquely detected in each of the three lectins.

the predominant  $Y_1$  ion along with its charged states, and therefore the mass of the core peptide. The observed peptide mass was then screened against the predicted masses of all peptides containing the *N*-linked glycosylation consensus motif from the previously identified glycoprotein list using our *in silico* script. The specifically matched candidate peptide sequence and its predicted y or b ion series were then compared with the existing MS/MS spectrum for confirmation of the correct assignment of peptide sequence and glycosylation site. Finally, once a peptide sequence was assigned and confirmed, the mass of the glycan was determined. The initial glycan composition was assessed using the web-based GlycoMod Tool software (39) and the glycan sequence was then determined by manual analysis of the remaining MS/MS fragment ions. This resulted in the structural characterization of 17 *N*-glycopeptides from 16 distinct glycoproteins in a single HILIC fraction that had a retention time of 20 min. Most of the identified glycopeptides had a single glycan structure attached, although four had two glycoforms and one had three. Importantly, we observed no particular pattern of glycan size, number or size of side chains, or other aspects of

glycan composition that correlated specifically with a particular lectin. The identification of the glycopeptides with their protein accession numbers, glycan sequences for each of the glycosylation sites and variable glycoforms are shown in Table I and supplemental Data S1. As expected, an overwhelming majority of identified glycopeptides had a typical complex type *N*-glycan comprising a pentose ( $\beta$  1–2 xylose) and/or deoxyhexose ( $\alpha$ -1,3-fucose) linked to the core  $\text{Man}_3\text{GlcNAc}_2$ . Fig. 4 shows an example of an MS/MS spectrum for the triple-charged precursor ( $m/z$  766.75 $^{3+}$ ), which was identified as the  $\text{Xyl}_1\text{Man}_3\text{GlcNAc}_2\text{Fuc}_1$  glycoform at the Asn residue of the tryptic peptide FSDKNFTLR, derived from the glycoprotein suberization-associated anionic peroxidase 1 (unigene, TU052308; NCBI accession number, P1500). This MS/MS spectrum provides direct evidence for the complex type *N*-linked glycosylation on the FSDKNFTLR peptide.

**Characterization of XEGIP *N*-glycan Structures and Endogenous Glycopeptides**—In the PI-IDA analysis, we found many MS/MS spectra for glycopeptides (containing all marker ions of typical glycan), but only ~10% could be assigned to a peptide sequence and so the number of *N*-glycopeptides

TABLE I  
*N*-glycan structures and the associated glycopeptides identified with different lectins

Lectin	Pfam <sup>a</sup>	Unigene	NCB <sup>b</sup>	Name	Glycopeptide	Structure <sup>c</sup>
ConA, GNA, LCH	GH 3	TU069753	CAN82161	Hypothetical protein	ILHLSDNNTTSIPR	
ConA, GNA, LCH	GH 38	TU004342	NP_189306	$\alpha$ -mannosidase, putative	NEFNITPR	
ConA, GNA, LCH	GH 38C	TU134197	ABG22500	Glycosyl hydrolase 38	QQFNVTPR	
ConA	GH 32N	TU043211	AAB30874	Acid invertase	TGVALVYETSNTSFK	
ConA	Pkinase	TU026176	BAK52390	Leucine rich repeat receptor protein kinase CLAVATA1	MGENYLNGSIPK	
GNA	Pkinase	TU036134	XP_002517029	Serine-threonine protein kinase	VTPQSITQINGNNTK	
GNA, LCH	Cyclase	TU019070	XP_002869098	Cyclase family protein	DKNLTADAMQSLHIPK	
ConA, GNA, LCH	Peroxidase	TU052308	P15003	Suberization-associated anionic peroxidase 1	FSDKNFTLR	
ConA, GNA	Peroxidase	TU032073	P15004	Suberization-associated anionic peroxidase 2	FSDKNFTVR	
ConA, GNA, LCH	Cu-oxidase	TU039462	XP_002532575	Multicopper oxidase, putative	METSIIINGTYR	
GNA	LRRNT_2	TU016973	ACM89597	Leucine rich repeat protein	INILNLSK	
ConA, GNA, LCH	LRRNT_2	TU041053	ABD46739	Leucine rich repeat protein	INILNLSK	
ConA, GNA, LCH	Aldose_epim	TU010189	AAL09397	Non-cell-autonomous protein pathway1	FTLNGTLYK	
ConA, GNA, LCH	Metallophos	TU035508	XP_003609435	Purple acid phosphatase-like protein	ISNIHYNVSGGDAYPV PDK	
ConA, GNA, LCH	DUF642	TU043529	CAB02653	Unknown	QILNVTKG	
ConA	DUF642	TU016878	CBI20999	Predicted protein	QILNVTK	
ConA	DUF642	TU016878	CBI20999	Predicted protein	ADLNGTEVLK	

<sup>a</sup> Protein family (<http://pfam.sanger.ac.uk>).

<sup>b</sup> NCBI accession numbers of the proteins identified during the manual interpretation of the *N*-glycopeptides.

<sup>c</sup> Glycan structures were determined by manual interpretation of MS/MS spectra as outlined in material and methods.

identified was relatively small. This reflects the labile nature of the glycan-peptide linkage and the fragile internal glycan bonds during CID, compared with peptide bonds, which often results in little or ambiguous information concerning peptide sequence. This problem is exacerbated by the low ionization efficiency, large mass, structural complexity and low abundance of *N*-glycopeptides (40, 41). A potential orthogonal, albeit low throughput, approach to confirm the glycosylation of candidate plant *N*-glycoproteins, as suggested by Buren *et al.* (42) is to structurally characterize purified recombinant forms that have been overexpressed in plant hosts. To determine the validity and potential of this approach, we selected a putative *N*-glycoprotein that we identified through both the

deglycosylation/deamidation study (supplemental Table S2) and the shotgun glycoprotein analysis (supplemental Table S1), but whose *N*-glycopeptide(s) and glycan compositions were not identified in the PI-IDA analysis (Table I). Specifically, we targeted the putative *N*-glycoprotein xyloglucan-specific endoglucanase inhibitor protein (XEGIP, AAN87262), a tomato protein that has been shown to inhibit the activity of a xyloglucan-specific endoglucanase (XEG) from *Aspergillus aculeatus* (43). Recombinant XEGIP was transiently expressed in *Nicotiana benthamiana* leaves as a fusion protein with a C-terminal TAP (tandem affinity purification) tag to facilitate purification. XEGIP has a predicted SP that is putatively cleaved between the residues 23 and 24 and has five predicted *N*-gly-



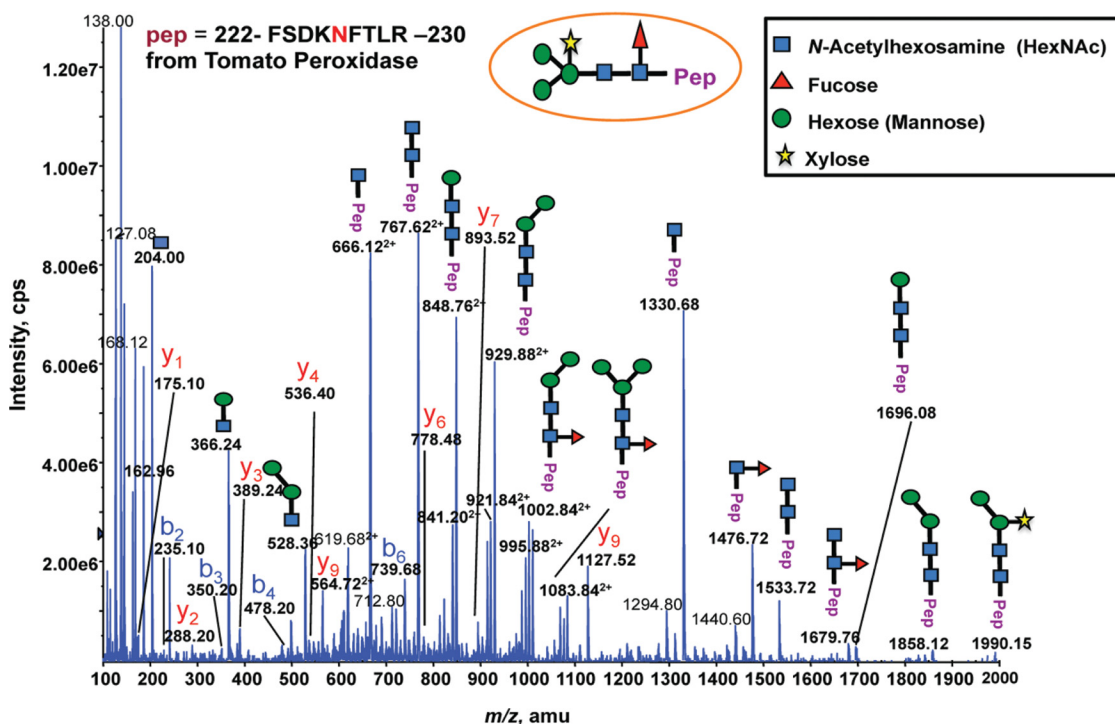


FIG. 4. MS/MS spectrum of an  $m/z$  766.75<sup>3+</sup> ion identifying the glycopeptide (FSDKNFTLR) from the tomato suberization-associated anionic peroxidase 1 (unigene, TU052308; NCBI accession number, P15003) by the selective PI scan triggered IDA approach. The spectrum revealed a typical “complex type” *N*-glycan representing a pentose ( $\beta$  1–2 xylose) and/or deoxyhexose ( $\alpha$  1–3 fucose) linked to the core Man<sub>3</sub>GlcNAc<sub>2</sub> structure.

cosylation sites (Fig. 5). MS analysis confirmed that the SP is indeed cleaved at the predicted site, as well as the presence of high mannose type *N*-glycans at four of the five predicted *N*-glycosylation sites (Table II, supplemental Data S2, supplemental Fig. S4). Considerable heterogeneity in glycan structures at each site was observed, with six glycoforms of ELAN<sub>322</sub>VTR and VVPIN<sub>279</sub>TLLSIDNQGVGGTK, five glycoforms of QTTCANFN<sub>423</sub>FTSID and four glycoforms of QN<sub>25</sub>QTSFRPK. We could not determine the presence of an *N*-glycan at N<sub>115</sub>TT, presumably because the size of the tryptic peptide that contains this glycosite is too large (60 amino acid residues; supplemental Fig. S3).

**Functional Annotation and Localization of *N*-glycoproteins**—In total, this MLAC profiling, together with the deglycosylation/deamidation and shotgun analyses, resulted in the identification of 578 *N*-glycoproteins from the tomato fruit pericarp. Of these, 348 were only identified using shotgun proteomics and 130 only using the deglycosylation strategy, whereas an additional 100 were identified through both strategies. Moreover, a comparison of arabidopsis homologs of the tomato glycoproteins identified in this current study and previous descriptions of arabidopsis *N*-glycoproteins (12, 44) (supplemental Fig. S3, supplemental Table S4) revealed substantial conservation of glycosylation status.

Given the site of *N*-glycosylation in the ER, *N*-glycoproteins would be expected to reside in one of the intracellular compartments or membranes of the secretory pathway (endo-

membrane system), or in the apoplast. We used PSORT and TargetP to predict the subcellular localization of all 578 putative *N*-glycoproteins and indeed 523 (90%) were predicted to be localized in the secretory pathway (Fig. 6A). However, some were predicted to be localized in other organelles (7.4% in the chloroplast, 0.3% in the nucleus and 0.5% in the mitochondrion), as well as 1.4% in the cytoplasm (Fig. 6A). Among all the predicted *N*-glycoproteins, the number of predicted glycosylation sites did not appear to correlate with predicted subcellular localization (Fig. 6A), although proteins with more than 10 such sites were only associated with the secretory pathway. Of the 523 proteins classified as in the secretory pathway, the majority (230; 44%) were predicted to be secreted to the apoplast, whereas the second most common location was the plasma membrane with 108 (21%) proteins having at least two transmembrane domains (Fig. 6B, supplemental Table S5).

The identified putative *N*-glycoproteins were grouped into families using Pfam, considering the highest bit score (24), and classified (Fig. 7) according to the functional classes of cell wall proteins proposed by Jamet *et al.* (25). The predominant functional group was ‘proteins acting carbohydrates’, of which 119 collectively represent 15 glycosyl hydrolase (GH) families, as well as 13 members of carbohydrate esterase family 8 (supplemental Table S4) and polysaccharide lyase family members. Most of these glycoproteins are related in cell wall restructuring and some have been well characterized,

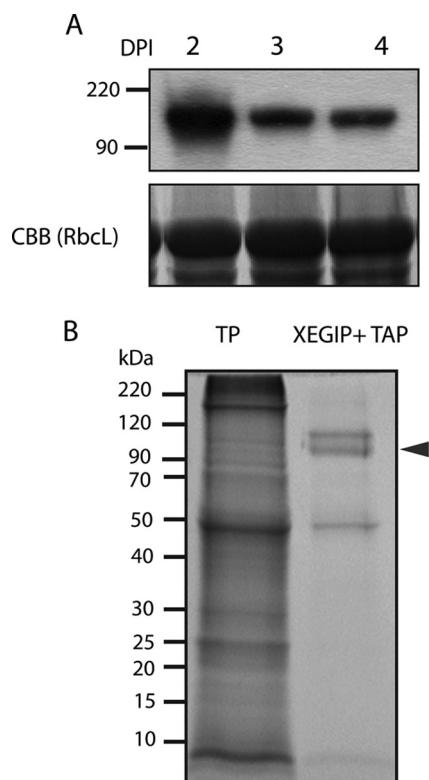


**FIG. 5. Transient expression and purification of recombinant xyloglucan-specific fungal endoglucanase inhibitor protein (XEGIP).** A, Western blot analysis (upper panel) using an anti-myc antiserum of proteins extracted from *N. benthamiana* leaves transiently expressing recombinant XEGIP fused to a Myc tag. Protein samples were extracted 2, 3, and 4 days post infiltration (DPI). Lower panel shows an image of the RuBisCO large subunit (Rbcl) protein in an SDS-PAGE gel stained with Coomassie brilliant blue (CBB), used as a loading control. B, SDS-PAGE gel (stained with CBB) of total protein (TP) from *N. benthamiana* leaves and a sample of the recombinant XEGIP+TAP after acidic elution from IgG beads, appearing as a double band (arrow).

such as polygalacturonase (GH28), endo-1,4- $\beta$ -glucanase (GH9) and xyloglucan endotransglucosylase/hydrolase (GH16) (25, 45, 46). The second largest class of *N*-glycoproteins (80; 14%) comprised predicted proteases, followed by proteins related to signaling events (73; 13%), oxido-reductases (46; 8%), proteins with protein interaction domains (39; 7%), and proteins related to lipid metabolism (24; 4%). We identified 30 *N*-glycoproteins with domains of unknown function (supplemental Table S4).

#### DISCUSSION

**Comparative Analysis of MLAC**—To date, the binding properties of ConA, GNA, and LCH have been evaluated using *N*-glycoproteins or *N*-glycopeptides derived from a range of eukaryotes, but with the notable exception of plants (47). Moreover, to our knowledge, there have not been any reports of a systematic comparison of glycoprotein populations that have been enriched using different lectins (8, 12, 13, 44, 48).

We therefore carried out a detailed comparative analysis of the *N*-glycoproteins associated with three mannose-binding lectin (ConA, GNA, and LCH), including the main three features of *N*-glycoproteins: the parent protein sequence, the amino acid residue composition and frequency at and around the *N*-glycosylation sites and the *N*-glycan structures associated with each lectin.

The data suggest that MLAC (combined ConA, GNA, and LCH) substantially increases the coverage of the plant *N*-glycoproteome compared with using single lectins (Fig. 2, supplemental Table S4). Significantly, although ConA is the most commonly used lectin for plant glycoprotein studies, only 54% of the total glycoproteins identified here were detected in the ConA binding fraction. Analysis of the amino acid frequency around the identified *N*-glycosylation sites (Fig. 3C) revealed a general similarity to previous studies of other model organisms (4, 6, 10, 13), suggesting a broad conservation of the *N*-glycosylation sequon across the taxonomic range of eukaryotes, spanning yeast and mammals (49). Our data also suggest the value of using multiple, rather than single lectins using the deglycosylation and deamidation analysis (Fig. 3A) and differences were detected in the relative frequencies of certain amino acids at and around the *N*-glycosylation sequon when considering only the lectin specific glycopeptides (Fig. 3D). We suggest that the disproportionate presence of specific amino acid residues in the  $-1$  or  $+1$  subsites in glycopeptides associated with ConA, GNA, and LCH may reflect one of both of two scenarios. The first is that the residues at these subsites may influence the structural conformation of the glycosylation sites (50) and consequently the accessibility of *N*-glycan modifying enzymes during protein maturation and *N*-glycan trimming. This may in turn, result in differences in *N*-glycan structures at the site variants that then differentially bind to the various lectins. A second explanation is that these sequon variants are associated with the same *N*-glycan structures, but differences in the structural conformation of the protein around the *N*-glycosylation site alter the specificity and/or avidity of the binding to those glycans to the various lectins. It is known that the presence of P at the  $+1$  subsite abolishes *N*-glycosylation (50, 51), whereas the presence of certain residues at this site can be associated with low or high glycosylation efficiency (52, 53). However, it is not known whether particular amino acid residues are key determinants of interactions with specific lectins.

Although our data clearly support the hypothesis that the differential binding of specific glycopeptides to particular lectins is driven by the unique composition, sequence and structural characteristics of the glycopeptides involved, it should be pointed out that the depth of coverage of the *N*-glycoproteome reported here is quite low. An alternative possibility is that apparent differential binding is a sampling artifact, although there is no compelling evidence to support this alternate hypothesis. A resolution of these opposing views could be addressed by a rigorous statistical analysis, which would

TABLE II  
*N*-glycans identified in the recombinant xyloglucan-specific endoglucanase inhibitor protein (XEGIP)

Peptide sequence	Glycan composition	Mass of glycan	RT (min)	m/z	z	M+H	Peptide+H
ELANVTR	(Hex) <sub>4</sub> (HexNAc) <sub>2</sub>	1054.36	10.97	928.90	2	1856.80	802.44
ELANVTR	(Hex) <sub>5</sub> (HexNAc) <sub>2</sub>	1216.36	10.97	1009.90	2	2018.80	802.44
ELANVTR	(Hex) <sub>6</sub> (HexNAc) <sub>2</sub>	1378.36	10.97	1090.90	2	2180.80	802.44
ELANVTR	(Hex) <sub>7</sub> (HexNAc) <sub>2</sub> *	1540.36	10.97	1171.90	2	2342.80	802.44
ELANVTR	(Hex) <sub>8</sub> (HexNAc) <sub>2</sub> *	1702.36	10.97	835.60	3	2504.80	802.44
ELANVTR	(Hex) <sub>9</sub> (HexNAc) <sub>2</sub> *	1863.76	10.97	889.4	3	2666.20	802.44
QNQTSFRPK	(Hex) <sub>6</sub> (HexNAc) <sub>2</sub>	1378.12	11.36	822.80	3	2466.40	1088.28
QNQTSFRPK	(Hex) <sub>7</sub> (HexNAc) <sub>2</sub>	1540.12	11.36	876.80	3	2628.40	1088.28
QNQTSFRPK	(Hex) <sub>8</sub> (HexNAc) <sub>2</sub> *	1702.12	11.36	930.80	3	2790.40	1088.28
QNQTSFRPK	(Hex) <sub>9</sub> (HexNAc) <sub>2</sub> *	1540.12	11.36	984.80	3	2952.40	1088.28
VVPINTLLSIDNQGVGGTK	(Hex) <sub>4</sub> (HexNAc) <sub>2</sub>	1054.08	21.49	1027.40	3	3080.20	2026.12
VVPINTLLSIDNQGVGGTK	(Hex) <sub>5</sub> (HexNAc) <sub>2</sub>	1216.08	21.49	1081.40	3	3242.20	2026.12
VVPINTLLSIDNQGVGGTK	(Hex) <sub>6</sub> (HexNAc) <sub>2</sub>	1378.38	21.49	1135.50	3	3404.50	2026.12
VVPINTLLSIDNQGVGGTK	(Hex) <sub>7</sub> (HexNAc) <sub>2</sub> *	1540.68	21.49	1189.60	3	3566.80	2026.12
VVPINTLLSIDNQGVGGTK	(Hex) <sub>8</sub> (HexNAc) <sub>2</sub> *	1702.68	21.49	1243.60	3	3728.80	2026.12
VVPINTLLSIDNQGVGGTK	(Hex) <sub>9</sub> (HexNAc) <sub>2</sub>	1864.08	21.49	1297.40	3	3890.20	2026.12
QTTCANFNFTSIDdpaflyk	(Hex) <sub>5</sub> (HexNAc) <sub>2</sub>	1216.42	25.57	1190.50	3	3569.50	2353.08
QTTCANFNFTSIDdpaflyk	(Hex) <sub>6</sub> (HexNAc) <sub>2</sub>	1378.12	25.57	1244.40	3	3731.20	2353.08
QTTCANFNFTSIDdpaflyk	(Hex) <sub>7</sub> (HexNAc) <sub>2</sub>	1540.72	25.57	1298.60	3	3893.80	2353.08
QTTCANFNFTSIDdpaflyk	(Hex) <sub>8</sub> (HexNAc) <sub>2</sub> <sup>a</sup>	1702.12	25.57	1352.40	3	4055.20	2353.08
QTTCANFNFTSIDdpaflyk	(Hex) <sub>9</sub> (HexNAc) <sub>2</sub> <sup>a</sup>	1864.42	25.57	1406.50	3	4217.50	2353.08

<sup>a</sup> High abundant glycoforms. The *N*-glycans and glycoforms were identified by nanoLC-PI scan (+204) triggered IDA analysis. Lower case letters in the peptide sequences refer to amino acid residues in the TAP tag fusion.

require a much greater depth of coverage of the *N*-glycoproteome; a fact that, in and of itself, should motivate additional experiments of the type reported here. Additional support for our hypothesis can be amassed by examining the retention of particular glycopeptides known to exhibit specific compositions and structures, a process that is made possible by recent advances in chemical synthesis and NMR characterization (54).

We did not observe particular glycan structural features associated with unique lectins (Table I), although the analysis was based on a relatively small number of *N*-glycans, reflecting the technical challenges associated with analyses at this scale (2, 40, 41). It is often difficult to obtain reliable information from direct MS analysis of glycopeptides even with relatively enriched glycopeptide samples, because of the labile nature of the glycan-peptide bond and the relatively fragile internal glycan bonds. The high level of fragmentation from glycan moieties and few fragment ions from the core peptide during traditional CID typically results in little, or ambiguous, information concerning peptide sequence, which exacerbates the already difficult process of determining the glycosylation site and glycan sequence. Another particular challenge is the large dynamic range of glycoproteins in biological samples, which means that low abundance glycoproteins are extremely difficult to detect in complex protein mixtures. This is already evident in the broad range of banding intensities using SDS-PAGE (Fig. 2A) and SYPRO ruby staining and the true range is, of course, even greater. To validate the robustness of our analytical pipeline and illustrate the high dynamic range of *N*-glycoproteins in our tomato fruit glycoprotein extracts, we

targeted a putative glycoprotein (XEGIP), which we identified by both shotgun sequencing and deglycosylation and deamidation analysis, but whose glycosylation abundance appeared so low that the constituent glycopeptides were not detected. We expressed XEGIP as a recombinant protein in tobacco leaves, purified the recombinant form and determined the presence and structure of the *N*-glycans (Table II). We confirmed that the protein is indeed glycosylated and our analysis further showed substantial glycan heterogeneity at the various predicted glycosylation sites. It is possible that at least some of the observed heterogeneity can be caused by artifacts associated with overexpression in a related species. However, earlier reports concerning the characterization of recombinant plant glycoproteins expressed in *N. benthamiana* and other plant species show similar *N*-linked oligosaccharides structures to those produced from the native species: high-mannose type *N*-glycans containing a core Man<sub>3</sub>HexNAc<sub>2</sub> substituted with two to six mannose residues, and complex type *N*-glycans present at β,1-2 xylose and/or α,1-3 fucose linked to the core (14, 55, 56, 57). Furthermore, we have previously reported a comparative characterization of *N*-linked glycosylation for HA protein from the H1N1 virus overexpressed in both *N. benthamiana* and insect cells (18). Overall similar glycosylation patterns were observed for all 5 identified *N*-linked glycosylation sites in both expression systems, which were similar to the patterns observed here. Thus, there is much empirical evidence to support the notion that the glycosylation of an overexpressed tomato protein accurately reflects the glycosylation status of the native tomato protein. It is noteworthy that only few glycoproteomic studies

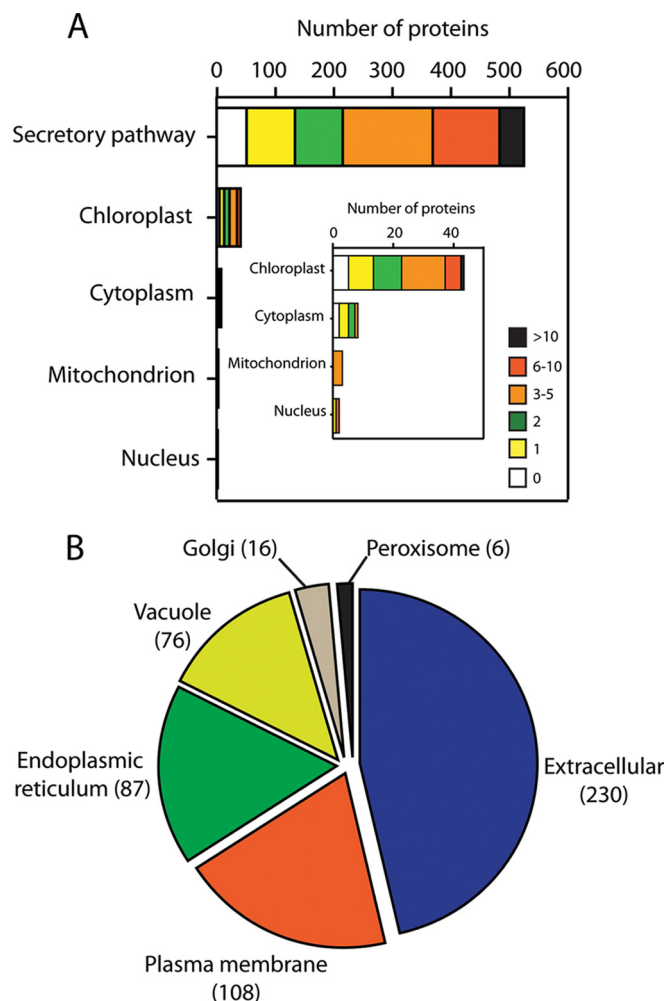


FIG. 6. **Subcellular location of identified *N*-glycoproteins.** *A*, the subcellular localizations were predicted with PSORT and TargetP. The numbers of predicted *N*-glycosylation sites in glycoproteins are indicated. *B*, predicted subcellular location of identified *N*-glycoproteins associated with the secretory pathway.

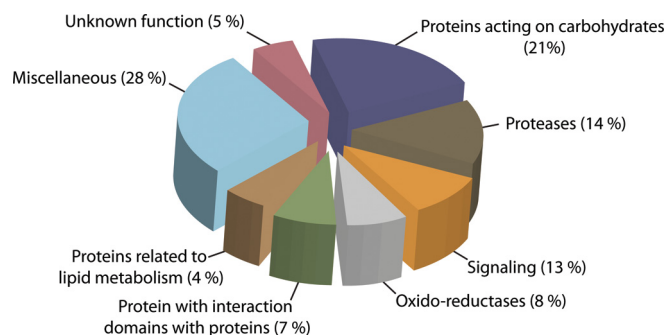


FIG. 7. **Functional classification of identified *N*-glycoproteins.** *N*-glycoproteins were grouped into families using the Pfam data base (24) and functionally classified according to Jamet et al. (25).

to date have determined the detailed structures and structural variants of *N*-glycans from plant *N*-glycoproteins (5, 58, 59).

*MLAC Provides an Overview of the Diversity of Glycoprotein Functions and Subcellular Localizations*—Bioinformatic anal-

ysis suggests that most (65%) of the *N*-glycoproteins identified in this study are located in the plant apoplast/cell wall or reside at the cell surface in the plasma membrane (Fig. 6B) and most of these are functionally classified as “proteins acting on carbohydrates” (Fig. 7, supplemental Table S5). This reflects the substantial cell wall assembly, remodeling and disassembly that is associated with fruit development and ripening and that has been extensively studied in tomato fruit (60–63). Although such studies have provided much information about the expression, regulation activities and endogenous substrates of wall modifying proteins such as polygalacturonase (PG, GH 28; supplemental Table S4), pectin methyl-esterase (PME, CE8; supplemental Table S4), xyloglucan endo-transglucosylase/hydrolases (XTHs) (XTH1 [Q40144], XTH3 [AAS46241], XTH7 [AAS46243], and XTH23 [XP\_002274827], supplemental Table S4) and expansins (AAD13631, AAD13632, and AAD13633, supplemental Table S4), almost nothing is known about the nature, extent, dynamics of functional significance of their *N*-glycosylation. The same applies to the *N*-glycoproteins that are predicted to localize in the plasma membrane, most of which are classified as having a signaling function (Fig. 7, supplemental Table S5). Several of the *N*-glycoproteins in this group are annotated as having a protein kinase domain and some are defined as receptor-like kinases (RLKs). Some plants RLKs have recognizable lectin domains and subsets are thought to bind to pectin in the cell wall (64, 65) where they may play a role in biomechanical sensing (66, 67). Several plant receptor kinases have potential *N*-glycosylation sites and it has been suggested that glycosylation may influence their function, stability, and transportation to the cell surface (66, 68). In this study, we characterized the protein and *N*-glycan structures of 5 glycopeptides derived from glycoproteins with protein kinase domain (Table I). Among this group, we observed two *N*-glycoforms of the peptide MGENYLN<sub>415</sub>GSIPK that corresponded to the leucine rich repeat receptor protein kinase CLAVATA1 (BAK52390, Table I). Interestingly, the tomato homolog of CLAVATA1 detected in our study (TU026176, Table I) has an *N*-glycosylated site, as confirmed by the identification of the glycopeptide MGENYLN<sub>415</sub>GSIPK, in the predicted extracellular domain (UniProt feature identifier: PRO\_0000403352). Thus, we were able to identify both soluble *N*-glycoproteins, and those that are at the cell surface and have glycans that are likely in intimate contact with the wall matrix.

A growing body of evidence suggests that *N*-glycoproteins can be located in the chloroplast (69, 70), an organelle that is not part of the canonical secretory pathway. Indeed, proteomic analysis of the arabidopsis chloroplast has provided supporting evidence that there are many proteins (>8% of total chloroplast proteome) with a predicted SP for ER translocation (71). Moreover, proteins such as a carbonic anhydrase (CAH1) from arabidopsis, and both a pyrophosphatase/phosphodiesterase and an  $\alpha$ -amylase from rice, have been shown to traffic through the ER to the Golgi apparatus (GA) and then to the chloroplast (72–74). Recently, complete char-

acterization of the structures of the *N*-glycans of CAH1 showed that blocking the *N*-glycosylation of this protein disrupts its transport to the chloroplast and enzymatic activity, highlighting the importance of *N*-glycosylation in its localization (42). Our data further support the existence the chloroplastic location of *N*-glycoproteins (73, 74, 32); however, experimental evidence is needed to corroborate their subcellular location *in vivo*. The detection of putative mitochondrial and nuclear *N*-glycoproteins in our study (Fig. 6) similarly warrants further investigation and underscores the potential value of MLAC as a platform for not only cataloging plant *N*-glycoproteomes, but also for providing insights into protein trafficking and localization.

\* This work has been supported by grants from the National Science Foundation Plant Genome Program (DBI-0606595), the USDA (1907-21000-37-00D), and the New York State Office of Science, Technology and Academic Research (NYSTAR).

§ This article contains supplemental Tables S1 to S6, Figs. S1 to S4 and Data S1 and S2.

|| To whom correspondence should be addressed: 412 Mann Library Building, Department of Plant Biology, Cornell University, Ithaca NY 14853. Tel.: +1-6072554781; E-mail: jr286@cornell.edu.

## REFERENCES

- Ruiz-May, E., Kim, S. J., and Rose, J. K. (2012) The secreted plant *N*-glycoproteome and associated secretory *Front. Plant Sci.* **3**, 117
- Ruiz-May, E., Thannhauser, T. W., Zhang, S., and Rose, J. K. (2012) Analytical technologies for identification and characterization of the plant *N*-glycoproteome. *Front. Plant Sci.* **3**, 150
- Song, W., Henquet, M. G., Mentink, R. A., van Dijk, A. J., Cordewener, J. H., Bosch, D., America, A. H., and van der Krol, A. R. (2011) *N*-glycoproteomics in plants: perspectives and challenges. *J. Proteomics* **74**, 1463–1474
- Zielinska, D. F., Gnad, F., Wisniewski, J. R., and Mann, M. (2010) Precision mapping of an *in vivo* *N*-glycoproteome reveals rigid topological and sequence constraints. *Cell* **141**, 897–907
- Halim, A., Nilsson, J., Ruetschi, U., Hesse, C., and Larson, G. (2012) Human urinary glycoproteomics; attachment site specific analysis of *N*- and *O*-linked glycosylations by CID and ECD. *Mol. Cell. Proteomics* **11**, M111 013649
- Breidenbach, M. A., Palaniappan, K. K., Pitcher, A. A., and Bertozzi, C. R. (2012) Mapping yeast *N*-glycosites with isotopically recoded glycans. *Mol. Cell. Proteomics*, M111.015339
- Choi, E., Loo, D., Dennis, J. W., O'Leary, C. A., and Hill, M. M. (2011) High-throughput lectin magnetic bead array-coupled tandem mass spectrometry for glycoprotein biomarker discovery. *Electrophoresis* **32**, 3564–3575
- Catala, C., Howe, K. J., Hucko, S., Rose, J. K., and Thannhauser, T. W. (2011) Towards characterization of the glycoproteome of tomato (*Solanum lycopersicum*) fruit using concanavalin A lectin affinity chromatography and LC-MALDI-MS/MS analysis. *Proteomics* **11**, 1530–1544
- Nilsson, C. L. (2011) Lectin techniques for glycoproteomics. *Curr. Proteomics* **8**, 248–256
- Kaji, H., Kamiie, J., Kawakami, H., Kido, K., Yamauchi, Y., Shinkawa, T., Taoka, M., Takahashi, N., and Isobe, T. (2007) Proteomics reveals *N*-linked glycoprotein diversity in *Caenorhabditis elegans* and suggests an atypical translocation mechanism for integral membrane proteins. *Mol. Cell. Proteomics* **6**, 2100–2109
- Mislovicova, D., Katrlík, J., Paulovicova, E., Gemeiner, P., and Tkac, J. (2012). Comparison of three distinct ELLA protocols for determination of apparent affinity constants between Con A and glycoproteins. *Colloids and surfaces. B. Biointerfaces.* **94**, 163–169
- Minic, Z., Jamet, E., Negroni, L., Arsene der Garabedian, P., Zivy, M., and Jouanin, L. (2007) A sub-proteome of *Arabidopsis thaliana* mature stems trapped on Concanavalin A is enriched in cell wall glycoside hydrolases. *J. Exp. Bot.* **58**, 2503–2512
- Zielinska, D. F., Gnad, F., Schropp, K., Wisniewski, J. R., and Mann, M. (2012) Mapping *N*-glycosylation sites across seven evolutionarily distant species reveals a divergent substrate proteome despite a common core machinery. *Mol. Cell* **46**, 542–548
- Nagels, B., Van Damme, E. J., Pabst, M., Callewaert, N., and Weterings, K. (2011) Production of complex multiantennary *N*-glycans in *Nicotiana benthamiana* plants. *Plant Physiol.* **155**, 1103–1112
- Tomato Genome Consortium (2012) The tomato genome sequence provides insights into fleshy fruit evolution. *Nature* **485**, 635–641
- Ding, W., Nothaft, H., Szymanski, C. M., and Kelly, J. (2009) Identification and quantification of glycoproteins using ion-pairing normal-phase liquid chromatography and mass spectrometry. *Mol. Cell Prot.* **8**, 2170–2185
- Varki, A., Cummings, R. D., Esko, J. D., Freeze, H. H., Stanley, P., Marth, J. D., Bertozzi, C. R., Hart, G. W., and Etzler, M. E. (2009) Symbol nomenclature for glycan representation. *Proteomics* **9**, 5398–5399
- Zhang, S., Sherwood, R. W., Yang, Y., Fish, T., Chen, W., McCardle, J. A., Jones, R. M., Yusibov, V., May, E. R., Rose, J. K., and Thannhauser, T. W. (2012) Comparative characterization of the glycosylation profiles of an influenza hemagglutinin produced in plant and insect hosts. *Proteomics* **12**, 1269–1288
- Lopez-Casado, G., Covey, P. A., Bedinger, P. A., Mueller, L. A., Thannhauser, T. W., Zhang, S., Fei, Z., Giovannoni, J. J., and Rose, J. K. (2012) Enabling proteomic studies with RNA-Seq: The proteome of tomato pollen as a test case. *Proteomics* **12**, 761–774
- Rubio, V., Shen, Y., Saijo, Y., Liu, Y., Gusmaroli, G., Dinesh-Kumar, S. P., and Deng, X. W. (2005) An alternative tandem affinity purification strategy applied to Arabidopsis protein complex isolation. *Plant J.* **41**, 767–778
- Sainsbury, F., Thuenemann, E. C., and Lomonosoff, G. P. (2009) pEAQ: versatile expression vectors for easy and quick transient expression of heterologous proteins in plants. *Plant Biotechnol. J.* **7**, 682–693
- Petersen, T. N., Brunak, S., von Heijne, G., and Nielsen, H. (2011) SignalP 4.0: discriminating signal peptides from transmembrane regions. *Nat. Methods* **8**, 785–786
- Helenius, A., and Aebi, M. (2004) Roles of *N*-linked glycans in the endoplasmic reticulum. *Annu. Rev. Biochem.* **73**, 1019–1049
- Punta, M., Coghill, P. C., Eberhardt, R. Y., Mistry, J., Tate, J., Boursnell, C., Pang, N., Forslund, K., Ceric, G., Clements, J., Heger, A., Holm, L., Sonnhammer, E. L., Eddy, S. R., Bateman, A., and Finn, R. D. (2011) The Pfam protein families database. *Nucleic Acids Res.* D290–D301
- Jamet, E., Canut, H., Boudart, G., and Pont-Lezica, R. F. (2006) Cell wall proteins: a new insight through proteomics. *Trends Plant Sci.* **11**, 33–39
- Nakai, K., and Horton, P. (1999) PSORT: a program for detecting sorting signals in proteins and predicting their subcellular localization. *Trends Biochem. Sci.* **24**, 34–36
- Emanuelsson, O., Brunak, S., von Heijne, G., and Nielsen, H. (2007) Locating proteins in the cell using TargetP, SignalP and related tools. *Nat. Protoc.* **2**, 953–971
- Krogh, A., Larsson, B., von Heijne, G., and Sonnhammer, E. L. (2001) Predicting transmembrane protein topology with a hidden Markov model: application to complete genomes. *J. Mol. Biol.* **305**, 567–580
- Hirokawa, T., Boon-Chieng, S., and Mitaku, S. (1998) SOSUI: classification and secondary structure prediction system for membrane proteins. *Bioinformatics* **14**, 378–379
- Schneider, T. D., and Stephens, R. M. (1990) Sequence logos - a new way to display consensus sequences. *Nucleic Acids Res.* **18**, 6097–6100
- Atwood, J. A., 3rd, Sahoo, S. S., Alvarez-Manilla, G., Weatherly, D. B., Kolli, K., Orlando, R., and York, W. S. (2005) Simple modification of a protein database for mass spectral identification of *N*-linked glycopeptides. *Rapid Commun. Mass Spectrom.* **19**, 3002–3006
- Kitajima, A., Asatsuma, S., Okada, H., Hamada, Y., Kaneko, K., Nanjo, Y., Kawagoe, Y., Toyooka, K., Matsuoka, K., Takeuchi, M., Nakano, A., and Mitsui, T. (2009) The rice alpha-amylase glycoprotein is targeted from the golgi apparatus through the secretory pathway to the plastids. *Plant Cell* **21**, 2844–2858
- Leiter, H., Mucha, J., Staudacher, E., Grimm, R., Gloszl, J., and Altmann, F. (1999) Purification, cDNA cloning, and expression of GDP-L-Fuc:Asn-linked GlcNAc alpha1,3-fucosyltransferase from mung beans. *J. Biol. Chem.* **274**, 21830–21839
- Wilson, I. B., Rendic, D., Freilinger, A., Dumic, J., Altmann, F., Mucha, J., Muller, S., and Hauser, M. T. (2001) Cloning and expression of cDNAs

- encoding alpha1,3-fucosyltransferase homologues from *Arabidopsis thaliana*. *Biochim. Biophys. Acta* **1527**, 88–96
35. Palmisano, G., Melo-Braga, M. N., Engholm-Keller, K., Parker, B. L., and Larsen, M. R. (2012) Chemical deamidation: a common pitfall in large-scale N-linked glycoproteomic mass spectrometry-based analyses. *J. Proteom. Res.* **11**, 1949–1957
  36. Ritchie, M. A., Gill, A. C., Deery, M. J., and Lilley, K. (2002) Precursor ion scanning for detection and structural characterization of heterogeneous glycopeptide mixtures. *J. Am. Soc. Mass Spectrom.* **13**, 1065–1077
  37. Zhang, S., and Williamson, B. L. (2005) Characterization of protein glycosylation using chip-based nano electrospray with precursor ion scanning quadrupole linear ion trap mass spectrometry. *J. Biomol. Tech.* **16**, 209–219
  38. Segu, Z. M., and Mechref, Y. (2010) Characterizing protein glycosylation sites through higher-energy C-trap dissociation. *Rapid Commun. Mass Spectrom.* **24**, 1217–1225
  39. Cooper, C. A., Gasteiger, E., and Packer, N. H. (2001) GlycoMod—a software tool for determining glycosylation compositions from mass spectrometric data. *Proteomics* **1**, 340–349
  40. An, H. J., Froehlich, J. W., and Lebrilla, C. B. (2009) Determination of glycosylation sites and site-specific heterogeneity in glycoproteins. *Curr. Opin. Chem. Biol.* **13**, 421–426
  41. Ytterberg, A. J., and Jensen, O. N. (2010) Modification-specific proteomics in plant biology. *J. Proteomics* **73**, 2249–2266
  42. Buren, S., Ortega-Villasante, C., Blanco-Rivero, A., Martinez-Bernardini, A., Shutova, T., Shevela, D., Messinger, J., Bako, L., Villarejo, A., and Samuelsson, G. (2011) Importance of post-translational modifications for functionality of a chloroplast-localized carbonic anhydrase (CAH1) in *Arabidopsis thaliana*. *PLoS One* **6**, e21021
  43. Qin, Q., Bergmann, C. W., Rose, J. K. C., Saladie, M., Kolli, V. S. K., Albersheim, P., Darvill, A. G., and York, W. S. (2003) Characterization of a tomato protein that inhibits a xyloglucan-specific endoglucanase. *Plant J.* **34**, 327–338
  44. Zhang, Y., Giboulot, A., Zivy, M., Valot, B., Jamet, E., and Albenne, C. (2010) Combining various strategies to increase the coverage of the plant cell wall glycoproteome. *Phytochemistry* **72**, 1109–1123
  45. Jamet, E., Albenne, C., Boudart, G., Irshad, M., Canut, H., and Pont-Lezica, R. (2008) Recent advances in plant cell wall proteomics. *Proteomics* **8**, 893–908
  46. Cosgrove, D. J. (2005) Growth of the plant cell wall. *Nat. Rev. Mol. Cell Biol.* **6**, 850–861
  47. Gabius, H. J., Siebert, H. C., Andre, S., Jimenez-Barbero, J., and Rudiger, H. (2004) Chemical biology of the sugar code. *ChemBiochem* **5**, 740–764
  48. Albenne, C., Canut, H., Boudart, G., Zhang, Y., San Clemente, H., Pont-Lezica, R., and Jamet, E. (2009) Plant cell wall proteomics: mass spectrometry data, a trove for research on protein structure/function relationships. *Mol. Plant* **2**, 977–989
  49. Lehle, L., Strahl, S., and Tanner, W. (2006) Protein glycosylation, conserved from yeast to man: a model organism helps elucidate congenital human diseases. *Angew Chem.* **45**, 6802–6818
  50. Imperiali, B., O'Connor, S. E., Hendrickson, T., and Kellenberger, C. (1999) Chemistry and biology of asparagine-linked glycosylation. *Pure Appl. Chem.* **71**, 777–787
  51. Bause, E. (1983) Structural requirements of N-glycosylation of proteins. Studies with proline peptides as conformational probes. *Biochem. J.* **209**, 331–336
  52. Mazola, Y., China, G., and Musacchio, A. (2011) Integrating bioinformatics tools to handle glycosylation. *PLoS Comput. Biol.* **7**, e1002285
  53. Shakin-Eshleman, S. H., Spitalnik, S. L., and Kasturi, L. (1996) The amino acid at the X position of an Asn-X-Ser sequon is an important determinant of N-linked core-glycosylation efficiency. *J. Biol. Chem.* **271**, 6363–6366
  54. Kang, J., Low, W., Norberg, T., Meisenhelder, J., Hansson, K., Stenflo, J., Zhou, G. P., Imperiali, J., Olivera, B. M., Rigby, A. C., and Craig, A. G. (2004) Total chemical synthesis and NMR characterization of the glycopeptide tx5a, a heavily post-translationally modified conotoxin, reveals that the glycan structure is alpha-D-Gal-(1->3)-alpha-D-GalNAc. *Eur. J. Biochem.* **271**, 4939–4949
  55. Balen, B., and Krsnik-Rasol, M. (2007) N-glycosylation of recombinant therapeutic glycoproteins in plant systems. *Food Technol. Biotech.* **45**, 1–10
  56. Ashraf, S., Singh, P. K., Yadav, D. K., Shah Nawaz, M., Mishra, S., Sawant, S. V., and Tuli, R. (2005) High level expression of surface glycoprotein of rabies virus in tobacco leaves and its immunoprotective activity in mice. *J. Biotechnol.* **119**, 1–14
  57. Fitchette, A. C., Dinh, O. T., Faye, L., and Bardor, M. (2007) Plant proteomics and glycosylation. *Methods Mol. Biol.* **355**, 317–342
  58. Kuroguchi, M., Matsushita, T., Amano, M., Furukawa, J., Shinohara, Y., Aoshima, M., and Nishimura, S. (2010) Sialic acid-focused quantitative mouse serum glycoproteomics by multiple reaction monitoring assay. *Mol. Cell. Proteomics* **9**, 2354–2368
  59. Kuroguchi, M., Amano, M., Fumoto, M., Takimoto, A., Kondo, H., and Nishimura, S. (2007) Reverse glycoblotting allows rapid-enrichment glycoproteomics of biopharmaceuticals and disease-related biomarkers. *Angew Chem. Int. Ed. Engl.* **46**, 8808–8813
  60. Rose, J. K., and Bennett, A. B. (1999) Cooperative disassembly of the cellulose-xyloglucan network of plant cell walls: parallels between cell expansion and fruit ripening. *Trends Plant Sci.* **4**, 176–183
  61. Brummell, D. A. (2006) Cell wall disassembly in ripening fruit. *Funct. Plant Biol.* **33**, 103–119
  62. Vicente, A. R., Saladie, M., Rose, J. K. C., and Labavitch, J. M. (2007) The linkage between cell wall metabolism and fruit softening: looking to the future. *J. Sci. Food Agric.* **87**, 1435–1448
  63. Seymour, G. B., Chapman, N. H., Chew, B. L., and Rose, J. K. (2012) Regulation of ripening and opportunities for control in tomato and other fruits. *Plant Biotechnol. J.* DOI: 10.1111/j.1467-7652.2012.00738.x.
  64. Kohorn, B. D., Johansen, S., Shishido, A., Todorova, T., Martinez, R., Defeo, E., and Obregon, P. (2009) Pectin activation of MAP kinase and gene expression is WAK2 dependent. *Plant J.* **60**, 974–982
  65. Decreux, A., and Messiaen, J. (2005) Wall-associated kinase WAK1 interacts with cell wall pectins in a calcium-induced conformation. *Plant Cell Physiol.* **46**, 268–278
  66. Cheung, A. Y., and Wu, H. M. (2011) THESEUS 1, FERONIA and relatives: a family of cell wall-sensing receptor kinases? *Curr. Opin. Plant Biol.* **14**, 632–641
  67. Steinwand, B. J., and Kieber, J. J. (2010) The role of receptor-like kinases in regulating cell wall function. *Plant Physiol.* **153**, 479–484
  68. Furukawa, K., Ohkawa, Y., Yamauchi, Y., Hamamura, K., and Ohmi, Y. (2012) Fine tuning of cell signals by glycosylation. *J. Biochem.* **151**, 573–578
  69. Gaikwad, A., Tewari, K. K., Kumar, D., Chen, W., and Mukherjee, S. K. (1999) Isolation and characterisation of the cDNA encoding a glycosylated accessory protein of pea chloroplast DNA polymerase. *Nucleic Acids Res.* **27**, 3120–3129
  70. Asatsuma, S., Sawada, C., and Kitajima, A. (2005) Investigation of intracellular localization of rice alpha-amylase isoforms. *Plant Cell Physiol.* **46**, S107
  71. Kleffmann, T., Russenberger, D., von Zychlinski, A., Christopher, W., Sjölander, K., Gruijssem, W., and Baginsky, S. (2004) The *Arabidopsis thaliana* chloroplast proteome reveals pathway abundance and novel protein functions. *Curr. Biol.* **14**, 354–362
  72. Jarvis, P. (2008) Targeting of nucleus-encoded proteins to chloroplasts in plants. *New Phytol.* **179**, 257–285
  73. Villarejo, A., Buren, S., Larsson, S., Dejardin, A., Monne, M., Rudhe, C., Karlsson, J., Jansson, S., Lerouge, P., Rolland, N., von Heijne, G., Grebe, M., Bako, L., and Samuelsson, G. (2005) Evidence for a protein transported through the secretory pathway en route to the higher plant chloroplast. *Nat. Cell Biol.* **7**, 1224–1231
  74. Nanjo, Y., Oka, H., Ikarashi, N., Kaneko, K., Kitajima, A., Mitsui, T., Munoz, F. J., Rodriguez-Lopez, M., Baroja-Fernandez, E., and Pozueta-Romero, J. (2006) Rice plastidial N-glycosylated nucleotide pyrophosphatase/phosphodiesterase is transported from the ER-golgi to the chloroplast through the secretory pathway. *Plant Cell* **18**, 2582–2592